Sensitivity of Age-of-Air Calculations to the Choice of Advection Scheme

Janusz Eluszkiewicz

Atmospheric and Environmental Research, Inc., Cambridge, Massachusetts

Richard S. Hemler and Jerry D. Mahlman

NOAA/Geophysical Fluid Dynamics Laboratory, Princeton, New Jersey

Lori Bruhwiler

NOAA/Climate Monitoring and Diagnostics Laboratory, Boulder, Colorado

Lawrence L. Takacs

Data Assimilation Office, Goddard Space Flight Center, Greenbelt, Maryland

ABSTRACT

The age of air has recently emerged as a diagnostic of atmospheric transport unaffected by chemical parameterizations, and the features in the age distributions computed in models have been interpreted in terms of the models' large-scale circulation field. This study shows, however, that in addition to the simulated large-scale circulation, three-dimensional age calculations can also be affected by the choice of advection scheme employed in solving the tracer continuity equation. Specifically, using the $3.0°$ latitude $\times 3.6°$ longitude and 40 vertical level version of the Geophysical Fluid Dynamics Laboratory SKYHI GCM and six online transport schemes ranging from Eulerian through semi-Lagrangian to fully Lagrangian, it will be demonstrated that the oldest ages are obtained using the nondiffusive centered-difference schemes while the youngest ages are computed with a semi-Lagrangian transport (SLT) scheme. The centered-difference schemes are capable of producing ages older than 10 years in the mesosphere, thus eliminating the "young bias" found in previous age-of-air calculations.

At this stage, only limited intuitive explanations can be advanced for this sensitivity of age-of-air calculations to the choice of advection scheme. In particular, age distributions computed online with the National Center for Atmospheric Research Community Climate Model (MACCM3) using different varieties of the SLT scheme are substantially older than the SKYHI SLT distribution. The different varieties, including a noninterpolating-in-the-vertical version (which is essentially centered-difference in the vertical), also produce a narrower range of age distributions than the suite of advection schemes employed in the SKYHI model. While additional MACCM3 experiments with a wider range of schemes would be necessary to provide more definitive insights, the older and less variable MACCM3 age distributions can plausibly be interpreted as being due to the semi-implicit semi-Lagrangian dynamics employed in the MACCM3. This type of dynamical core (employed with a 60-min time step) is likely to reduce SLT's interpolation errors that are compounded by the short-term variability characteristic of the explicit centered-difference dynamics employed in the SKYHI model (time step of 3 min). In the extreme case of a very slowly varying circulation, the choice of advection scheme has no effect on two-dimensional (latitude–height) age-of-air calculations, owing to the smooth nature of the transport circulation in 2D models.

These results suggest that nondiffusive schemes may be the preferred choice for multiyear simulations of tracers not overly sensitive to the requirement of monotonicity (this category includes many greenhouse gases). At the same time, age-of-air calculations offer a simple quantitative diagnostic of a scheme's long-term diffusive properties and may help in the evaluation of dynamical cores in multiyear integrations. On the other hand, the sensitivity of the computed ages to the model numerics calls for caution in using age of air as a diagnostic of a GCM's large-scale circulation field.

1. Introduction

A concept that has gained wide popularity as a diagnostic of stratospheric transport is the mean age of air. For a tracer with no chemical sink whose tropospheric mixing ratio increases linearly with time, the mean age of air at a stratospheric location is usually identified as the lag time between the occurrence of a particular mixing ratio at this location and its occurrence in the troposphere. To date, the age of air has been determined using measurements of CO_2 (Bischof et al. 1985; Schmidt and Khedim 1991; Woodbridge et al. 1995; Daniel et al. 1996; Boering et al. 1996), SF_6 (Har-

Corresponding author address: Dr. Janusz Eluszkiewicz, Atmospheric and Environmental Research, Inc., 840 Memorial Dr., Cambridge, MA 02139.
E-mail: jel@aer.com

nisch et al. 1996), the CFCs (Pollock et al. 1992), and HF (Russell et al. 1996). Despite persisting uncertainties in these observational estimates, the ''age'' measurements are a source of information about stratospheric transport unaffected by chemistry. This is also true for mean age distributions computed in numerical models. The most direct way to compute the mean age of stratospheric air in a model is as an ensemble average of transit times for particles initialized in the troposphere (Kida 1983). Alternatively, the mean age can be computed by simulating a linearly increasing passive tracer (as in the observational studies referred to above) or as the first temporal moment of the age spectrum represented as a Green's function (Hall and Plumb 1994). Frequently, differences between mean age distributions computed by different models have been attributed to differences in wind fields, including wave breaking and the strength of the residual circulation (Hall and Waugh 1997; Waugh et al. 1997; Bacmeister et al. 1998; Hall et al. 1999; Neu and Plumb 1999).

However, age simulations, in addition to being influenced by a model's three-dimensional wind field and subscale closure schemes, also depend on the model's numerics. This is because age experiments consist of multiyear integrations of a passive tracer initialized in a localized portion of the atmosphere and the resulting distributions can be expected to be very sensitive to diffusion and dispersion errors inherent in the advection schemes used to solve the tracer continuity equation. At the same time, relatively little is known about the performance of various advection schemes in long three-dimensional integrations, as most schemes are usually tested in idealized 1D or 2D flows and short integrations (e.g., Mahlman and Sinclair 1977; Rood 1987; Williamson and Rasch 1989; Lin and Rood 1996), or in 3D simulations of atmospheric tracers affected by chemical and/or physical processes (with the models' chemical and physical parameterizations obscuring the intrinsic behavior of advection schemes). Moreover, prior to the advent of the age measurements, the only observational data against which the simulations of truly conservative tracers could be compared were the rather sparse radioactive carbon-14 and strontium-90 data from the nuclear bomb tests in the 1960s.

This paper will show that a wide range of mean age distributions can be obtained with the same wind field depending on the choice of tracer advection scheme, with the nondiffusive schemes generating the oldest ages. This will be demonstrated in the Geophysical Fluid Dynamics Laboratory (GFDL) SKYHI general circulation model, which can employ a wide range of contemporary advection schemes in solving the tracer continuity equation (SKYHI's suite of advection schemes includes a fully Lagrangian code that constitutes an end-member transport scheme with almost no numerical diffusion). The identified sensitivity of model ages to the choice of advection scheme thus calls for caution in interpreting age-of-air distributions as solely dependent on a model's large-scale transport behavior.

The organization of this paper is as follows. The background information about the SKYHI model, as well as about the Middle Atmosphere version of the National Center for Atmospheric Research (NCAR) Community Climate Model (MACCM3) and the Goddard Earth Observing System GCM (GEOS-2) (both of which have been employed in supporting numerical experiments), is presented in section 2. The age-of-air distributions obtained in experiments with linearly increasing tracer carried out with the SKYHI and MACCM3 models are the focus of section 3. This section also includes a brief discussion of age calculations in a 2D (latitude–height) chemical transport model. Comparisons of our GCM ages with available observations are presented in section 4. Section 5 discusses the behavior of the various transport schemes in shorter (seasonal) integrations with the SKYHI and GEOS-2 models. The paper concludes with a summary and discussion in section 6.

2. General circulation models

This section provides a brief overview of the GCMs employed in our numerical experiments, with particular emphasis on their dynamical formulation and the tracer advection schemes.

a. GFDL SKYHI model

The primary numerical experiments described in this paper have been performed with the GFDL SKYHI general circulation model (Fels et al. 1980; Hamilton et al. 1995). SKYHI's dynamical core is formulated on an unstaggered Arakawa A grid and uses 2d- and 4th-order centered differences in the horizontal and vertical dimensions, respectively. For the long-term integrations described in this paper, we have employed the $3.0° \times 3.6°$ version with 40 vertical levels. This version uses a 3-min time step.

1) ADVECTION SCHEMES

The SKYHI model can employ a variety of advection schemes to solve the Eulerian tracer continuity equations. The schemes have been implemented online; that is, the driving winds are available at every model time step. Four schemes have been implemented to date:

1) A centered-difference scheme that is 2d-order in the horizontal and 4th-order in the vertical (Mahlman and Moxim 1978).
2) A centered-difference scheme that is classified as pseudo–4th order. This scheme is ''pseudo–4th order'' because the horizontal advecting velocities are obtained using a 2d-order scheme. In this form, the advective terms are both globally quadratic conserving and, in the parent GCM, nonlinearly stable (no

spurious cascade of globally integrated variance at smaller scales).

3) A hierarchy of finite-volume schemes developed by Lin and Rood (1996). In the age-of-air calculations to be described below, both monotonic and nonmonotonic versions of the Lin–Rood scheme have been adopted.

4) An advective-form semi-Lagrangian scheme developed by Rasch and Williamson (Rasch and Williamson 1990; Williamson and Rasch 1994) [''the semi-Lagrangian transport (SLT) scheme'']. The monotonic version with a mass conservation adjustment and Hermite cubic interpolation has been used. The required derivative estimates are obtained by differentiating a cubic Lagrange polynomial interpolant. These estimates are modified when necessary to produce a monotonic interpolant and thus a monotonic scheme.

Of the four schemes, the SLT scheme is computationally the most expensive for a single tracer, increasing the running time of the 3.0° version by about 30% (the other schemes add about 10% each). However, the incremental cost of the SLT scheme for additional tracers is less than for the other schemes.

SKYHI's parameterization of subgrid-scale diffusion, dependent on resolution and radius of deformation in the horizontal (Smagorinsky 1963; Andrews et al. 1983) and the Richardson number in the vertical (Levy et al. 1982), is designed to let the advective process determine where local mixing is appropriate, that is, where the flow deformation in the horizontal is large or when the vertical structure is convectively or dynamically unstable. These parameterizations are employed with the centered difference and the nonmonotonic Lin–Rood schemes; they are not used with the monotonic Lin–Rood and SLT schemes, which as will be shown below, are already overly diffusive. The choice of the coefficients is somewhat arbitrary but is designed to keep the variance in the smaller scales consistent with the observed mesoscale variance spectrum (Koshyk et al. 1999b). In that sense, the most successful SKYHI horizontal resolution is 1.0° × 1.2° (Strahan and Mahlman 1994); the 3.0° × 3.6° version (used here) is somewhat overdiffusive and the ⅓° × 0.4° version (Mahlman 1997) may be insufficiently diffusive (it should be noted that the coefficients have not been tuned for any particular resolution). The SKYHI horizontal and vertical diffusion parameterizations have an additional diffusion coefficient added in the circumstances where errors in advection lead to production of negative trace mixing ratios. Locally, diffusion is added to ''fill in'' the negative value (the filling is not used with the monotonic schemes). The net level of this formally diffusive process is always considerably smaller than the magnitude of net diffusion provided by the SKYHI subscale parameterization, but the term can dominate locally, for example, near a stationary source where the tracer gra-dients are very large. The presence of this term, which depends on mixing ratio gradients, makes the transport operator nonlinear in the tracer mixing ratio. This nonlinearity, albeit localized in space and time, affects the equivalence between lag time and age (Hall and Plumb 1994), but we will continue to use the two terms interchangeably.

2) TRAJECTORY CALCULATIONS

In addition to employing the gridded advection schemes described above, the age distributions in the SKYHI model have also been calculated using a fully Lagrangian (trajectory) code. Trajectories are computed by integrating the set of equations

$$\frac{d\mathbf{x}_i}{dt} = \mathbf{v}_i, \qquad \mathbf{x}_i \equiv (\lambda_i, \phi_i, z_i), \qquad i = 1, \dots, N, \quad (1)$$

where N is the total number of particles; (λ_i, ϕ_i, z_i) are the longitude, latitude, and vertical position (pressure or potential temperature) of the ith particle; and $\mathbf{v}$ is the three-dimensional wind at the instantaneous location of the particle, obtained by linear interpolation in space and time from a gridded velocity field generated by the model. The use of wind data from a free-running GCM maximizes their internal consistency, in contrast to wind data obtained by current four-dimensional assimilation techniques, which often produce unreliable vertical wind speed estimates (e.g., Weaver et al. 1993), unreliable ageostrophic winds, and problematic wind speed estimates in low latitudes. Our trajectory code has the option of using kinematic velocities or diabatic heating rates as vertical velocities. The kinematic velocities are defined as $\dot{\sigma} \equiv d\sigma/dt$, where σ is the hybrid coordinate used by the SKYHI model (Fels et al. 1980)

$$\sigma = \frac{p - p_c}{p^* - p_c} \qquad \text{for } p > p_c \quad \text{and}$$

$$\sigma = \frac{p - p_c}{1013.25 - p_c} \quad \text{for } p < p_c, \qquad (2)$$

with p^* being the surface pressure and $p_c = 353.55$ hPa. The diabatic heating rates, expressed here as the rate of change of potential temperature $\dot{\theta} \equiv d\theta/dt$, include contributions from radiative heating, latent heating, dry and moist convective adjustment, and subgrid-scale diffusion. The two kinds of trajectories will henceforth be referred to as ''$\dot{\sigma}$'' and ''$\dot{\theta}$'' trajectories.

The sampling frequency of the wind data used in the trajectory calculations can be set to any multiple of the model time step (3 min for the 3.0° × 3.6° version), with the option of performing calculations online (i.e., every model time step). Note that most published Lagrangian studies of stratospheric transport have been performed offline [the work of Mote et al. (1994) being one notable exception], that is, with winds sampled every few hours from independent meteorological anal-

yses (assimilation, GCM runs, etc.), thus either excluding or aliasing the effects of high-frequency processes. In addition, apart from the Mote et al. paper, past trajectory calculations have either been restricted to quasi-horizontal surfaces (isentropic or isobaric) or used potential temperature as the vertical coordinate and the rate of diabatic heating as the vertical velocity. In many cases, the heating rates have been calculated independently of the wind-generating model, thus raising questions about their consistency with the horizontal winds. Our trajectory code avoids such inconsistencies, thus allowing an in-depth investigation of the effect of the two choices for the vertical velocity. Of course, assimilated wind data do offer their own advantages, in particular the opportunity of analyzing actual weather events. However, since our study aims at elucidating fundamental aspects of long-term three-dimensional trajectory calculations, internal consistency of the wind field is more important than its correspondence with a particular set of observed flow patterns.

For the trajectory calculations reported in this paper, we have adopted the online approach. The rationale for this choice has been our desire to provide a "clean" comparison between $\dot{\sigma}$ and $\dot{\theta}$ trajectories. In our past research with the SKYHI model, we have discovered that sampling the winds every few hours in trajectory calculations (i.e., the usual offline approach) leads to spurious vertical transport caused by the aliasing of $\dot{\sigma}$ velocities, and we have chosen to eliminate this additional complication from the present work. On the other hand, by opting for the online approach, we have restricted ourselves to forward trajectories, as long integrations of backward trajectories only become practical offline.

b. Middle atmosphere version of the NCAR CCM3

The MACCM3 results quoted in this study were obtained from an unpublished model currently under development by F. Sassi and B. Boville (1999, personal communication). MACCM3 has been extensively modified from the tropospheric CCM3 described in Kiehl et al. (1996, 1998). MACCM3 adopts a semi-Lagrangian, semi-implicit spectral transform dynamical core, a variant of the scheme described in Williamson et al. (1998). Water vapor and constituent transport are also treated in a semi-Lagrangian manner. Biharmonic horizontal diffusion is applied to the dynamical variables but not to water vapor or other constituents. The MACCM3 employs a two-time level integration scheme. A three-time level version has also been used to allow noninterpolating-in-the-vertical approximations (see below). The MACCM3 suite of physical parameterizations includes a 9-component gravity wave spectrum parameterization. The version used for the simulations reported here is T63 spectral resolution, with an accompanying 2.8° linear Gaussian transform grid and 52 vertical levels (18 levels between the ground and 100 mb and an ex-

plicit lid at 0.001 mb). The model is integrated with a 60-min time step.

The details of the implementation of SLT scheme in the CCM3 are described in Kiehl et al. (1996). The scheme uses cubic Hermite interpolants, with the required derivative estimates obtained by differentiating a cubic Lagrange polynomial interpolant. These estimates are modified when necessary to produce a monotonic interpolant and thus a monotonic transport scheme. In addition to the standard monotonic version of the SLT, employed both with the two-time level and the three-time level dynamical cores, two other versions of semi-Lagrangian transport have also been used with the three-time level version. One is noninterpolating-in-the-vertical following Ritchie (1991) (the introduction of this version has necessitated the adoption of the three-time level integration scheme). The only difference from Ritchie's formulation is that if the departure point falls within the first grid interval on either side of the arrival point, the "Lagrangian" point is chosen to be the arrival point rather than the grid point closest to the departure point. Because of the time step used, this means that except in rare instances, the vertical tracer advection is nominally second-order, centered Eulerian, as in the Eulerian dynamics. A "filler" (local in vertical and longitude) is used to eliminate the negative mixing ratios generated by this scheme. This scheme will allow us to study the impact of an essentially nondiffusive vertical transport on the computed ages. In the other variant of the SLT scheme, the time step for tracer transport is 6 min, that is, 10 times shorter than the dynamical time step. In this variant, the dynamical time step is used to calculate the trajectories, while the departure points are based on the shorter time step. This version will allow us to test whether the frequency of interpolations can have an effect on the computed ages.

c. GEOS-2 model

The GEOS general circulation model has been developed by the Data Assimilation Office at the Goddard Laboratory for Atmospheres (Schubert et al. 1993; Takacs et al. 1994). Version 2 of the GEOS dynamical core (GEOS-2) adopted in the current experiments employs the Sadourney energy and potential enstrophy conserving scheme (Burridge and Haseler 1977), which provides 4th-order accuracy for the advection of 2d-order vorticity by the nondivergent part of the flow. Horizontal advection of potential temperature, moisture, and passive tracers is performed using the 4th-order scheme in use in the University of California, Los Angeles, GCM (A. Arakawa 1995, personal communication). In addition to the standard 4th-order scheme, the GEOS-2 model can also advect tracers using the Lin–Rood hierarchy of schemes and the NCAR SLT scheme has been incorporated for this paper. A Shapiro (1970) filter is used to damp small-scale features in the dynamical and tracer fields (the filter is not used for tracers advected with the

Lin–Rood and SLT schemes). In order to reduce the dynamical imbalances generated by an intermittent use of the full filter, a filter tendency is defined to incorporate only a fraction of the full filter at each model time step, with the filter timescale chosen so as to remove the two-grid interval wave in 6 h.

It should be noted that the GEOS-2 model belongs to the same model class as SKYHI in its use of an explicit, finite-difference dynamics and short time steps, the major numerical difference being that GEOS-2 is formulated on a C grid, while SKYHI uses an unstaggerered A grid. An effort has been made to match the resolution of the GEOS-2 and SKYHI runs by adopting for the GEOS-2 model an experimental version of 3.0° latitude × 3.6° longitude and 42 vertical levels between surface and 0.01 hPa, and a time step of 3 min.

3. Meridional age distributions

a. SKYHI

Using the gridded advection schemes, the mean ages have been computed by simulating the evolution of a passive tracer whose mixing ratios are specified to increase linearly with time at the bottom four levels of the 40-level model [see Fig. 2.1 of Fels et al. (1980) for the definition of SKYHI vertical levels], with the mean age defined as the asymptotic lag time between a given location and the surface. In our experiments, these asymptotic values were obtained after about 20 model years for the centered-difference schemes, but for the SLT scheme the ages were already established after 5 model years. In the trajectory approach, the age of stratospheric air at any particular location (defined by an Eulerian box) has been computed directly from the distribution of transit times (the time elapsed since the entry into the stratosphere) for particles in that box (Kida 1983). Ideally, the particles should have been initialized at the surface, but the computational cost of doing so would be prohibitive, since most particles would then be confined to the troposphere. Instead, the particles are initialized close to the tropical tropopause, between 1.5°S and 1.5°N in the upper half of the vertical layer bounded by the 103- and 82-hPa pressure levels, at the rate of one particle every 15 min, with the longitudinal, meridional, and vertical positions within the source region chosen by means of a random number generator. To further ease the computational burden, particles are removed from the calculations when they enter the troposphere, with the local tropopause defined as in Eluszkiewicz (1996) using the model-generated distribution of nitrous oxide. It is believed that in the region above 100 hPa, which is populated by particles entering through the tropical tropopause, this procedure leads to a uniform and small offset relative to ages referenced to a surface source (see discussion below). As in the linear tracer experiment, about 20 model years were required to establish a statistical steady-state (i.e., the

total number particles not changing in the stratosphere in the annual mean), with the transit times of a very large number particles (>2 million) used in the computation of annual mean ages.

The zonal and annual mean distributions of age obtained using the gridded schemes, and the $\dot{\sigma}$ and $\dot{\theta}$ trajectories are shown in Fig. 1. The integrations have been performed online with the GCM (time step 3 min), and the ages are relative to the tropical tropopause. For the gridded distributions, the age relative to the tropopause has been set equal to the difference between the age relative to the surface and the zonal mean age at the tropopause relative to the surface. The age at the tropopause ranges from 0.2 to 0.4 yr depending on advection scheme, close to the 0.5 years obtained by Waugh et al. (1997) and somewhat shorter than the 0.8 years inferred by Volk et al. (1997). In the trajectory approach, the mean ages are relative to the tropical tropopause by design and they have been computed as averages of transit times for particles in Eulerian boxes 10° latitude × 2 km altitude. The number of particles in each box decreases with altitude, but even in the highest boxes close to the stratopause the numbers are sufficient (100 or more) to assure robust statistics.

The choice of transport scheme has a clear impact on the computed ages. The distributions obtained using the centered-difference schemes have the oldest ages and are most vertically stratified. The distributions computed using $\dot{\theta}$ trajectories and the nonmonotonic Lin–Rood scheme are also vertically stratified but are progressively younger than for the centered-difference schemes. The $\dot{\sigma}$ trajectories produce young and old air in the Tropics and high latitudes, respectively, with a peaked distribution characterized by weak vertical gradients in the subtropics and midlatitudes. The distribution obtained with the SLT scheme is at the opposite extreme to the distributions computed using centered-difference schemes: its gradients are very weak and the ages are very young.

Figure 1 shows that in the middle and upper stratosphere the nonmonotonic Lin–Rood scheme produces ages about 3 yr younger than the ages produced by the 2d-/4th-order scheme. Still younger ages are produced when monotonic versions of the Lin–Rood scheme are employed. The effect of monotonicity for the Lin–Rood scheme on the age-of-air calculations is illustrated in Fig. 2, which shows distributions computed using various combinations of monotonic and nonmonotonic schemes in the horizontal and vertical dimensions (see caption for details). The fully monotonic Lin–Rood scheme produces ages that are only about 2 yr older than the SLT distribution in Fig. 1.

We note that the distributions shown in Fig. 1 span the morphological classes introduced by Hall et al. (1999): the centered-difference and the Lin–Rood distributions belong to Hall et al.'s "class C," the $\dot{\sigma}$ distribution to "class B," and the SLT distribution to "class A." Hall et al. argue that a "peaked" distribution (i.e.,
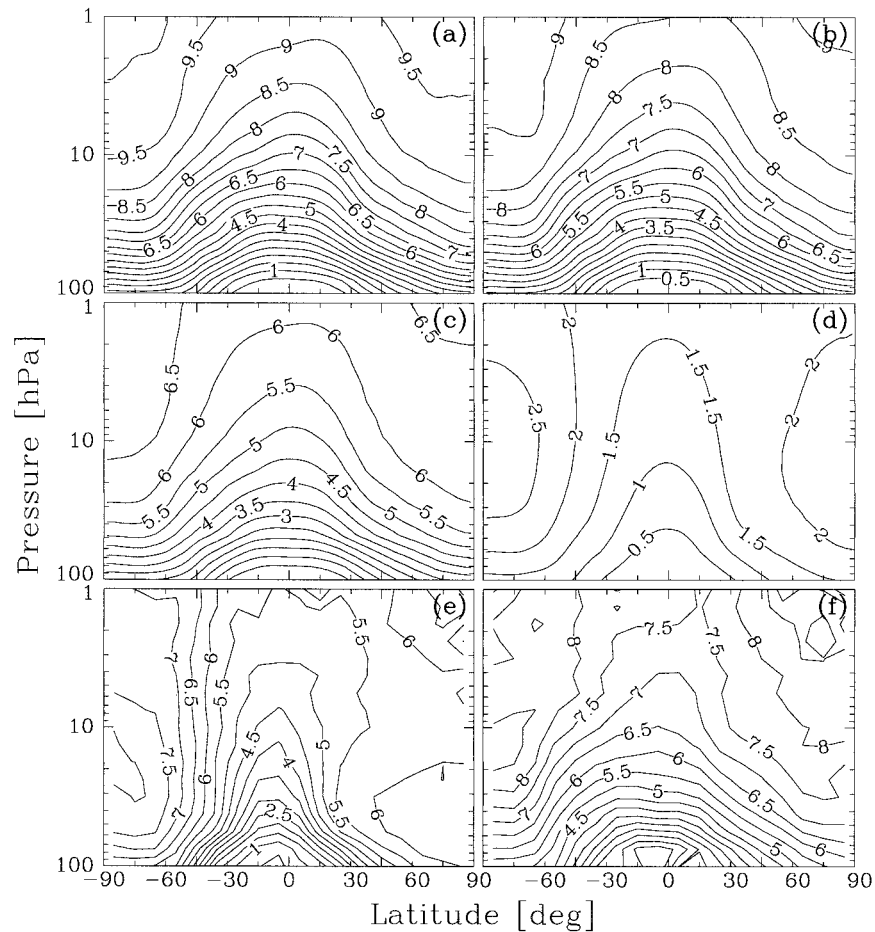
FIG. 1. Zonal and annual mean age distributions computed online with the SKYHI model using (a) 2d-/4th-order scheme, (b) pseudo–4th-order scheme, (c) nonmonotonic Lin–Rood scheme, (d) NCAR SLT scheme, (e) $\dot{\sigma}$ trajectories, and (f) $\dot{\theta}$ trajectories. Contour interval is 0.5 yr. The ages are inferred as the lag times relative to the source for a linearly increasing tracer and are plotted relative to the tropical tropopause. See text for detailed information on the schemes and on the experimental setup.

classes A and B) indicates isolation of the Tropics from midlatitudes [the "tropical pipe" paradigm of Plumb (1996)], while a class C distribution is more consistent with the "global diffuser" paradigm (Holton 1986; Mahlman et al. 1986), in which horizontal mixing is global in extent. In view of the present results, however, we believe that in addition to the degree of tropical isolation (and other characteristics of large-scale transport), an at least equally important role in shaping 3D age distributions can be played by the choice of advection scheme.

In section 4 we will use observational age estimates to provide qualitative insights into which scheme produces the most realistic ages. However, already at this stage it seems possible to make a preliminary assessment. The distribution based on $\dot{\theta}$ trajectories is probably closer to the "ground truth" for the model than that produced using $\dot{\sigma}$ trajectories. This is because $\dot{\theta}$ trajectories utilize smoothly varying diabatic heating

rates and require several months to transport material across the height of a vertical grid box (≈ 2 km). This transport rate is consistent with the rate inferred from measurements of water vapor in the tropical lower stratosphere [the so-called tape recorder signal (Mote et al. 1996)]. On the other hand, although $\dot{\sigma}$ trajectories utilize the model's detailed vertical velocities and are capable, in principle, of resolving subgrid-scale transport, they suffer from interpolation errors that cause their rate of vertical transport to be too fast, even in online calculations (see section 5a).

If the age distribution based on $\dot{\theta}$ trajectories is indeed accepted as being closer to the ground truth for the model than are the $\dot{\sigma}$ trajectories, then the similarity between the $\dot{\theta}$-based distribution and the distributions obtained using centered-difference schemes means that the lack of numerical diffusion for the latter schemes outweighs their dispersion errors in this application. The $\dot{\theta}$ distribution actually gives somewhat younger ages
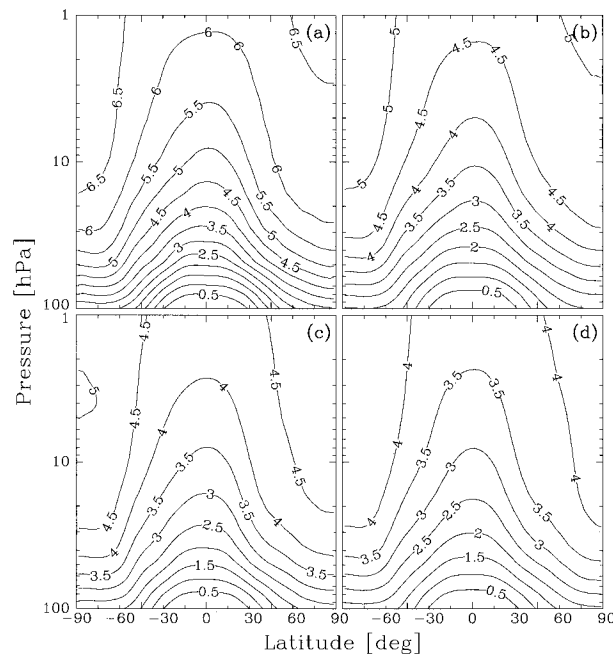
FIG. 2. Effect of monotonicity on the age calculations in the SKYHI model with the Lin–Rood scheme: (a) nonmonotonic scheme, i.e., in the notation of Lin and Rood (1996), FFSL-5, in all three dimensions, with the Smagorinsky parameterization employed to represent subgrid horizontal diffusion; (b) nonmonotonic in the horizontal, monotonic in the vertical (FFSL-5 and FFSL-3 in the horizontal and vertical directions, respectively); (c) monotonic in the horizontal, nonmonotonic in the vertical (FFSL-3 and FFSL-5, respectively, without the Smagorinsky parameterization); (d) monotonic (i.e., FFSL-3) in all three dimensions (without the Smagorinsky parameterization).
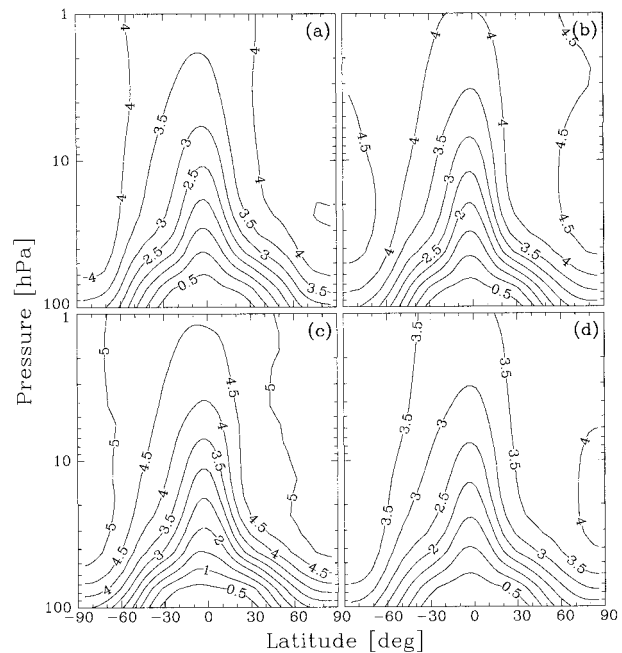

FIG. 3. Zonal and annual mean age distributions for the MACCM3. The four panels show distributions obtained with four versions of the SLT scheme: (a) monotonic (two-time level), (b) monotonic (three-time level), (c) noninterpolating-in-the-vertical, and (d) short–time step. The three-time level GCM has been employed to generating distributions (c) and (d). See text for details.

than the centered-difference schemes, but this could be related, at least in part, to the ambiguity caused by the differences in the location of the source region in the two experiments (tropopause vs surface). This ambiguity may be eliminated in future work by calculating age using backward trajectories. The nonmonotonic Lin–Rood distribution in Fig. 1c is somewhat more diffusive, with younger ages and weaker gradients than for the $\dot{\theta}$ distribution, but the scheme can still be considered "realistic" (the monotonic versions in Fig. 2b are progressively less realistic). In contrast, the SLT distribution is clearly unrealistic, being dominated by numerical diffusion. The distribution based on $\dot{\sigma}$ trajectories is a special case, looking "unrealistic" (in fact, the shape of its contours is similar to the SLT distribution), but for quite different reasons (see section 5a).

b. MACCM3

The age distributions from the MACCM3 experiment are shown in Fig. 3. Four versions of the SLT have been employed: standard monotonic of the two- and three-time level variety, non-interpolating-in-the-vertical, and short–time step (the latter two versions were employed in the three-time level fashion). Clearly, this suite of

advection schemes is not as comprehensive in terms of their diffusive properties as the schemes employed in the SKYHI model, but a consideration of even only this restricted range should help in putting the SKYHI results in a somewhat broader context. The distributions in Fig. 3 are substantially older than the SKYHI SLT distribution in Fig. 1d, but all four are peaked and still rather young. The noninterpolating-in-the-vertical version leads to slightly older ages compared with the monotonic scheme, confirming that numerical diffusion (which is surpressed in this version in the vertical direction) is responsible for generating young ages. On the other hand, shortening the time step for tracer transport leads to somewhat younger ages compared with the standard version, although the effect is not as drastic as in the SKYHI model. This suggests that the frequency of interpolations is only one factor contributing to the very young ages in SKYHI, with SKYHI's short-term dynamical variability being the other likely factor.

The distributions in Fig. 3 are qualitatively similar to the MONASH2 distribution obtained by Hall et al. (1999), who used SLT driven by time-averaged winds from an earlier version of the CCM, the MACCM2 (which employs a somewhat stronger variant of our 9-component gravity wave drag parameterization). This overall similarity demonstrates that the age distribution has been little affected either by the changes in wind fields between MACCM2 and MACCM3 or by the use of online versus time-averaged winds. We note, how-

ever, that the effect of time averaging is probably reduced in MACCM3 compared with SKYHI, as the former uses semi-Lagrangian dynamics and semi-implicit time differencing, both of which reduce short-term wind variability. Older ages have been computed by Hall and Waugh (1997), who used winds generated by a run of the MACCM2 with only the orographic gravity wave drag (the MONASH1 model). The MONASH1 ages are in fact close to those inferred from measurements, but this is most likely an artifact in view of the insufficient amount of drag and a sluggish meridional circulation. As discussed by Hall et al. (1999), most other 2D and 3D models exhibit a young bias. Without information about the models' meridional circulation it is impossible to determine the exact cause of this bias, but our SKYHI results strongly suggest that the choice of advection scheme may play a role in the 3D calculations. In particular, to our knowledge none of the previous 3D age calculations employed a nondiffusive advection scheme (a brief discussion of the "young bias" in 2D models is presented in section 3c). It is interesting to note that the MACCM2/SLT distribution obtained by Hall and Waugh (1997) was more peaked (albeit older) than the distribution they obtained using winds from the Goddard Institute for Space Studies' (GISS's) GCM and the second-moment scheme of Prather (1986). While Hall and Waugh attributed this result to the coarse spatial resolution of the GISS model, we speculate, in view of the present results, that the diffusive nature of the SLT scheme also played a role. This hypothesis is further strengthened by the fact that the numerical diffusion of the Prather scheme (often reputed to be "nondiffusive") is comparable to the numerical diffusion of the nonmonotonic Lin–Rood scheme [both schemes produce very similar age distributions in offline calculations based on winds from the GISS model (D. Rotman 1999, personal communication)]. Consequently, in view of the results shown in Fig. 1, we would expect the Prather scheme to generally produce a more stratified (and, for the same spatial resolution, older) age distribution than the SLT scheme.

c. "Young bias" in 2D models

As discussed by Hall et al. (1999), a "young bias" is characteristic of most models both in 3D and in 2D. While our SKYHI results demonstrate that for 3D models the cause of this bias might reside in the choice of advection scheme, the 2D zonally averaged chemical transport models utilize residual circulation and a parameterization of horizontal diffusion (the so-called K_{yy}'s) as the transport circulation and, in view of the slowly varying nature of this circulation we would expect the choice of advection scheme to be much less important in 2D. We have indeed confirmed this expectation using AER's 2D model (Weisenstein et al. 1998; Shia et al. 1998) and a variety of advection schemes, including a diffusive upstream scheme, the

scheme of Smolarkiewicz (1983), the second-moments scheme (Prather 1986), and a nondiffusive centered-difference scheme. For a wide range of residual circulations diagnosed from contemporary satellite data (Eluszkiewicz et al. 1996, 1997) and various assumptions about the K_{yy}'s, we have noticed no effect on the age calculations from the choice of advection scheme. Among the cases considered was the extreme case of $K_{yy} \equiv 0$, thus indicating that it is the smooth nature of the transport circulation, rather than explicit diffusion, that makes 2D age calculations insensitive to the choice of advection scheme. For commonly accepted choices of the K_{yy}'s, the ages were nowhere older than 6 yr, thus confirming the "young bias" relative to the observed ages (which are discussed in section 4). The only way to produce substantially older ages was by adopting values of the K_{yy}'s in excess of 10^{10} cm^2 s^{-1}, which is about an order of magnitude larger than commonly accepted values. With such large K_{yy}'s we obtained very flat distributions with ages older than 10 yr in the upper stratosphere [the ability of horizontal mixing to produce old ages in idealized models was noted by Neu and Plumb (1999)]. While such large K_{yy}'s could possibly be ruled out by inspecting the associated distributions of chemically reactive species (e.g., Shia et al. 1998), we note that such procedure would invalidate the concept of age as a diagnostic of transport unaffected by chemistry. Put another way, a wide range of age distributions can be obtained in a 2D model (including "old" distributions), but the realism of the transport circulations producing these distributions cannot be ascertained independently of chemical parameterizations.

4. Comparison with observations

The preliminary assessment of the realism of the various age distributions presented in section 3a is borne out by comparisons of the SKYHI results with observational estimates. In making these comparisons it should be kept in mind that the version of the SKYHI model used in this paper has a rather sluggish meridional circulation (manifested as the "cold pole" bias) that is likely to have generated an old bias in the age distribution (Hall et al. 1999). Moreover, although the tracer measurements from which age is inferred are highly accurate, there are significant uncertainties in the inferred ages, caused by the sporadic nature of the measurements, by ambiguity in inferring age relative to the tropopause for tracers whose growth rates are known from surface data, and by deviations from the assumption of linear growth (Volk et al. 1997). Because of these complications, only rather qualitative conclusions can be drawn from these comparisons (differences of less than ≈ 2 yr being probably insignificant). In principle, instead of computing age distributions, we could have computed the distribution of conservative tracers such as CO_2, assuming realistic time histories and geographical distributions of their sources, and compared this
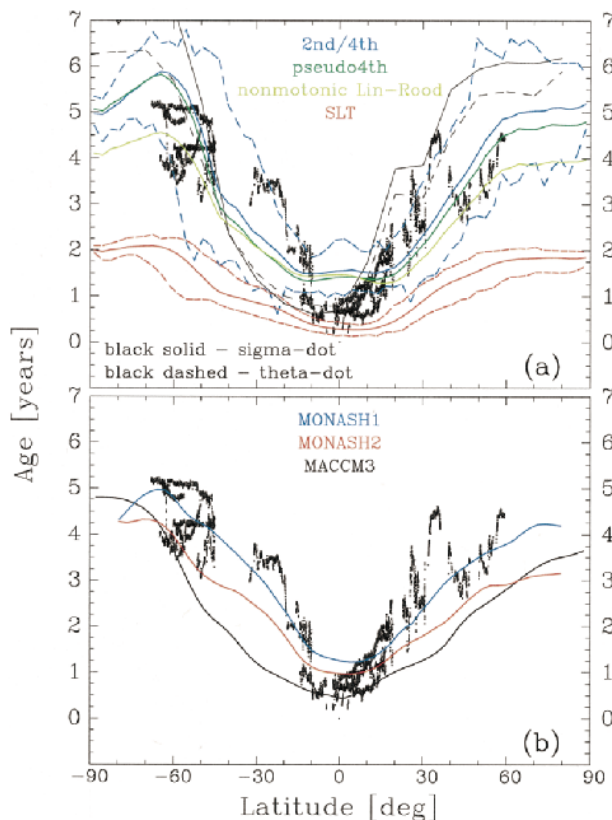
FIG. 4. Comparison of model zonal mean ages with ages inferred from the aircraft CO_2 measurements of Boering et al. (1996) at 19 km. In both panels, the measured ages are represented by dots. All ages are are for the Oct–Nov season and are relative to the tropical tropopause. (a) SKYHI ages obtained with six advection schemes. The dashed blue and red lines indicate the maximum and minimum values around a latitude circle for the 2d-/4th-order and SLT distributions. (b) Ages computed using the offline model based on NCAR MACCM2 winds without and with gravity wave drag (MONASH1 and MONASH2, respectively) and computed online with the MACCM3 using monotonic two-time level SLT. The MACCM2 results have been kindly provided by Darryn Waugh and are taken from Waugh et al. (1997) and Hall et al. (1999).

distribution directly with the measurements. Such experiments may be carried out in the future. On the other hand, it is likely that the concept of age in its idealized form adopted in this paper will continue to be useful both as a tool for comparing diverse models and datasets and as an intuitively appealing diagnostic of advection schemes (and possibly dynamical cores as well).

Figure 4 shows the latitudinal distribution of age at 19 km in October–November from the SKYHI model, from the MACCM2-based offline tracer model of Waugh et al. (1997) and Hall et al. (1999), and from our MACCM3 calculations. The model results are compared to ages inferred from the aircraft CO_2 measurements of Boering et al. (1996). All data are relative to the tropical tropopause and they pertain to the appropriate season, in contrast to the annual mean distributions shown in Fig. 1. While it is difficult to assign error

bars to the ages inferred from measurements, the good agreement between ages inferred from independent CO_2 and SF_6 measurements suggests uncertainty of less than 1 yr, at least in the lower and middle stratosphere (Hall et al. 1999). The model data in Fig. 4 represent zonal means, except the dashed blue and red lines that represent the maximum and minimum values around a latitude circle for the 2d-/4th-order and SLT schemes. The zonal variability for the SLT scheme ($\approx$0.5–1 yr) is comparable to that obtained by Waugh et al. (see their Fig. 10), but the variability for the 2d-/4th-order scheme is significantly larger. As shown by Strahan et al. (1994), the SKYHI model simulates the wintertime spatial variability in middle and high northern latitudes rather well.

Apart from the clearly unrealistic SLT generated ages, the SKYHI ages in Fig. 4a bracket the observations, as do the CCM ages in Fig. 4b. However, the agreement is less good for MONASH2 than for MONASH1 (recall that the MONASH2 model includes extra gravity wave drag), and the MACCM3 ages are younger still (especially in southern subtropics and midlatitudes). It should be noted that the MONASH models (which use the SLT scheme for tracer transport) are based on winds averaged in 6-h intervals. The success of MONASH1 in matching the observations, in contrast to the SKYHI SLT results in Fig. 4a, is probably due to time averaging as well as to differences in temporal and spatial differencing between the NCAR and GFDL models, with the short-term dynamical variability in the SKYHI model compounding the numerical diffusion due to interpolation errors in the SLT scheme.

In addition to the aircraft data in the lower stratosphere, there exist several profiles of age derived from balloon measurements of SF_6 (Harnisch et al. 1996). While restricted to a few locations, these data are valuable by extending into the middle stratosphere and thus providing an additional test for the models. A comparison of SKYHI zonal mean ages with the balloon measurements is shown in Fig. 5. We do not show a comparison with balloon observations of our MACCM3 ages, as the latter are close to the young MONASH2 ages discussed by Hall et al. (1999). In contrast to Fig. 4, ages plotted in Fig. 5 are relative to the surface, with the trajectory-derived ages computed relative to the surface by adding 0.8 yr to the results shown in Fig. 1 (the trajectory profiles are only valid above 16 km). This shift has been suggested by Volk et al. (1997), but obviously the magnitude of this shift in the model is uncertain and only qualitative conclusions can be drawn regarding the agreement between trajectory calculations and measurements in Fig. 5. Perhaps the most striking feature in Fig. 5 are the very young and clearly unrealistic ages in the SLT profiles. Above 25 km, the best agreement with observations is obtained with the centered-difference schemes and the $\dot{\theta}$ trajectories in high latitudes and with the nonmonotonic Lin–Rood scheme and $\dot{\sigma}$ trajectories in subtropics and midlatitudes. Below
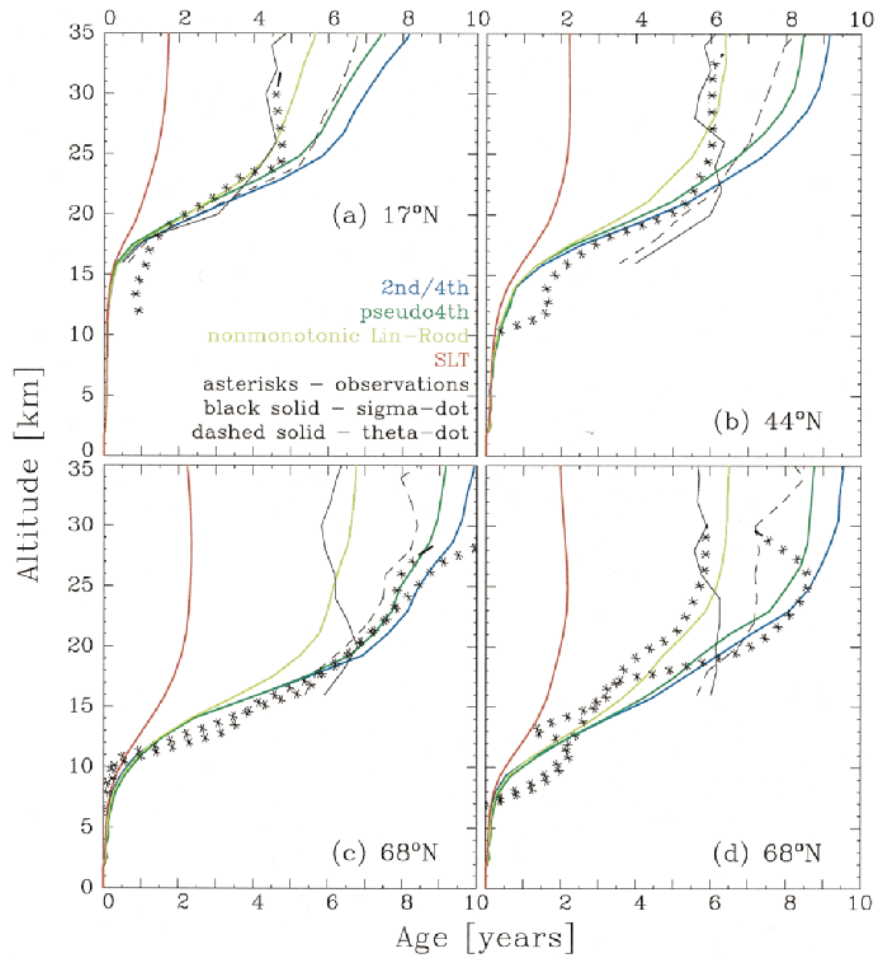
FIG. 5. Comparison of zonal mean ages computed in the SKYHI model with ages inferred from the balloon measurements of Harnisch et al. (1996) (asterisks). Observational ages have been interpolated to a regular grid. Observations and model results are for (a) 17°N (Mar), (b) 44°N (Sep), (c) 68°N (Jan–Feb), (d) 68°N (Mar). All ages are relative to the surface, with the trajectory-based ages referenced to the surface by adding 0.8 yr (Volk et al. 1997).

25 km, all non-SLT schemes produce a reasonable agreement with the data.

Finally, an important constraint on the age of air in the mesosphere has recently been provided by Harnisch et al. (1999), who used rocket measurements of the very long-lived compund CF_4 to infer an age of ≈ 11 yr between 56 and 61 km at 68° during late northern spring. This age is very similar to the age obtained in our SKY-HI experiments using the 2d–4th-order scheme. The other Eulerian schemes give progressively younger ages at this location: 10, 7, and 2 yr for the pseudo–4th-order, nonmonotonic Lin–Rood, and SLT schemes, respectively. While the close agreement between the 2d–4th-order results and measurements is probably fortuitous in view of the sluggish meridional circulation in the 3° version of SKYHI, these results nevertheless provide another demonstration that the least diffusive schemes produce most realistic ages, including ages older than 10 yr.

5. Short-term behavior

The different age distributions shown in Fig. 1 result from numerical factors already evident in shorter integrations. The purpose of this section is to present results from seasonal integrations, together with some attempts at explaining the observed behavior.

a. Trajectory distributions

The peaked age distribution obtained using $\dot{\sigma}$ trajectories (Fig. 1e) results from high-frequency vertical motions that, although essentially adiabatic, are numerically not constrained to the model θ surfaces. This is illustrated in Fig. 6, which shows particle positions after 120 days in the trajectory run used in generating Fig. 1. The $\dot{\sigma}$ particles undergo large vertical excursions that are inconsistent with the diabatic heating rates, both in the model and in the real atmosphere (judging by com-
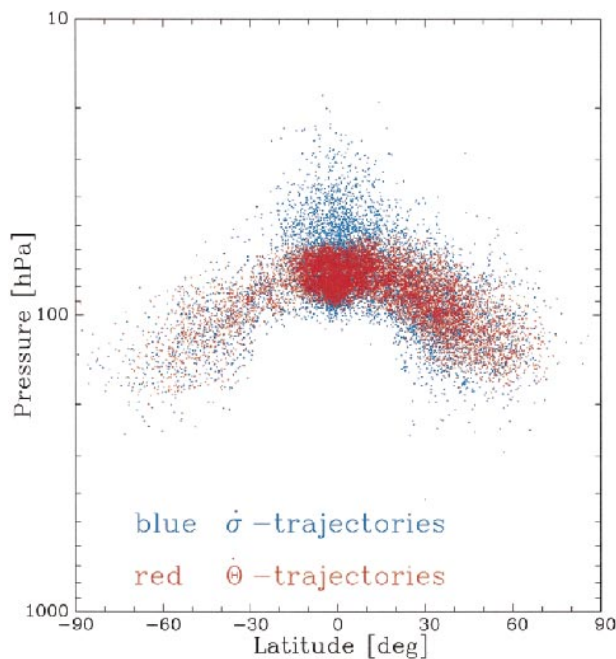
FIG. 6. Positions of particles initialized at the tropical tropopause after 120 days of a SKYHI run started on 1 Jan. See text for details of initialization. Blue and red dots represent particles advected with $\dot{\sigma}$ and $\dot{\theta}$ velocities, respectively. Note that some blue dots are obscured.

parison with the ascent rates inferred from the "tape recorder" signal in tropical water vapor data).

The presumably spurious cross-isentropic motions were noted previously in offline trajectory calculations by Eluszkiewicz et al. (1995), who speculated that they might be caused by the aliasing of kinematic velocities when the winds are sampled every few hours. The present results, obtained with an online code, demonstrate that this is not the likely explanation. These spurious motions are not eliminated by various computational enhancements, such as doubling of the vertical resolution in the dynamical module of the GCM or the use of a Runge–Kutta (rather than Euler forward) time-marching scheme in the trajectory code. In fact, increasing the vertical resolution to 80 levels seems to actually worsen the discrepancy between $\dot{\sigma}$ and $\dot{\theta}$ trajectories. These spurious motions appear thus to be intrinsic to $\dot{\sigma}$ trajectories, which do not recognize the location of isentropic surfaces at each trajectory time step. As a consequence, $\dot{\sigma}$ trajectories are unrealistic in long-term integrations. The most plausible explanation for this behavior is that it represents a random walk effect caused both by real physical processes (e.g., gravity waves) and by computational noise in the interpolated $\dot{\sigma}$ velocities. In addition, it is possible that the trilinear interpolation operator used in the trajectory calculations produces excessive numerical diffusion for the $\dot{\sigma}$ trajectories. The behavior of $\dot{\sigma}$ trajectories illustrates a basic inconsistency between the trajectory calculations and the Eulerian dynamics of SKYHI and other GCMs, caused by the inability of trajectory calculations based on $\dot{\sigma}$ to maintain reversibility (relative to isentropic surfaces) for adiabatic motions.

b. Eulerian and semi-Lagrangian distributions

The very young ages for the SLT scheme in Fig. 1d result from rapid vertical transport of tracer from the source region at the surface up into the middle stratosphere. While this is conceivably an artifact of the SKYHI numerics, rapid vertical transport was also seen in the work of Boville et al. (1991) and Mote et al. (1994), who used the SLT scheme in the MACCM2 to simulate the evolution of idealized tracers representing the aerosol cloud from the Mt. Pinatubo eruption. The work by Boville et al. focused on the horizontal spreading of the cloud, but they also showed the meridional cross sections, with significant amounts of tracer reaching 1 hPa in 60 days. This vertical transport is almost certainly too rapid, based on the radiative heating rates in the real world (Eluszkiewicz et al. 1996, 1997) and presumably also in the MACCM2. Even faster and clearly unrealistic vertical transport rates were obtained by Mote et al. (1994), who in their stratospheric Pinatubo-like simulations noted a rapid descent over a vertical distance of 10 km in a couple of days.

We have attempted to repeat the Boville et al. simulation using the four advection schemes and the trajectory code, and the results of our simulation are shown in Fig. 7 (the nonmonotonic Lin–Rood scheme has been used in these calculations). The Eulerian schemes advect material too rapidly in the vertical compared with the trajectory results, with the SLT scheme producing the most rapid transport. The similarity in the vertical extent of the distribution shown in Fig. 7d and that in Fig. 6a of Boville et al. demonstrates that the diffusive nature of the SLT scheme is not peculiar to the SKYHI model. On the other hand, it should be noted that rapid vertical spreading of a pointlike cloud was not present in the work of Rasch et al. (1994), who also performed simulations with the MACCM2, but at somewhat higher vertical resolution (44 levels vs 35 in Boville et al.). For example, in Fig. 2c of Rasch et al. the tracer has only moved to about 35 km in 45 days, whereas in Fig. 6a of Boville et al. the tracer is present close to the stratopause (50 km) after 60 days. This difference is probably attributable to vertical resolution. Unpublished Pinatubo-like simulations with the 52-level MACCM3 show a vertical extent similar to the non-SLT schemes in SKYHI. The limited vertical extent seems to be a rather robust feature of the MACCM3 runs, while the horizontal extent and maximum values for the plume are very dependent on the initial longitudinal location and date; that is, they exhibit a large amount of "natural" variability (however, the MACCM3 runs have much less horizontal spread of the structure at day 60 than either the SKYHI or the GOES-2 runs).
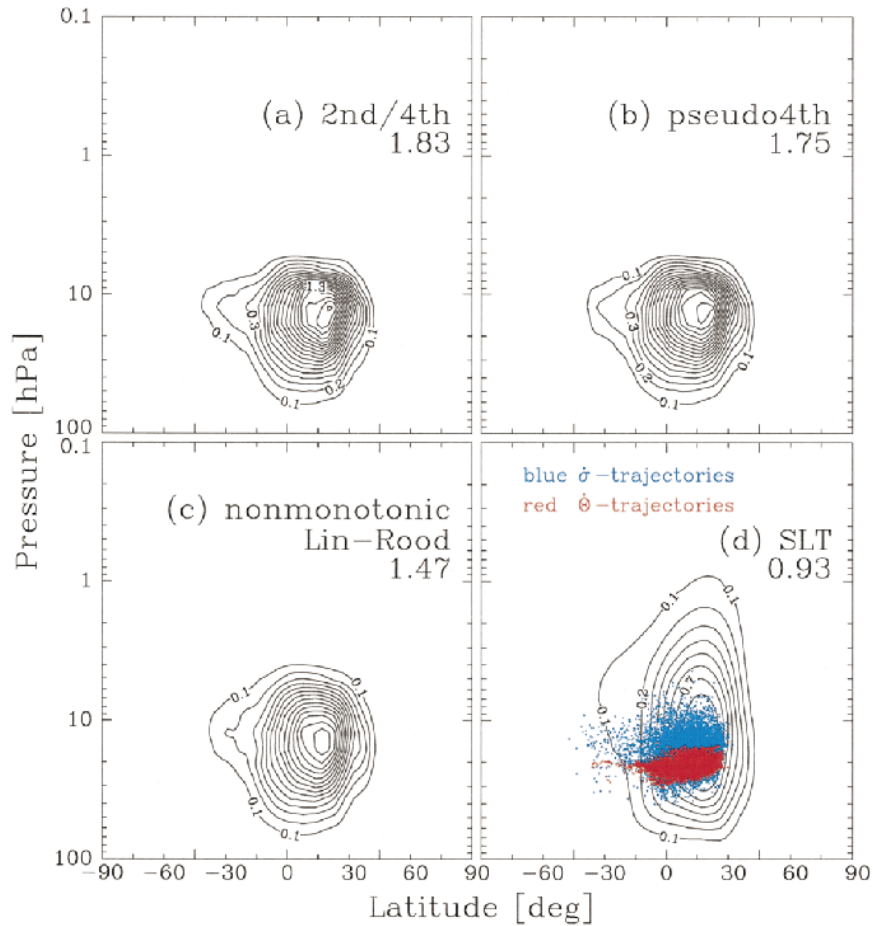
FIG. 7. SKYHI simulated distribution of a passive tracer representing aerosol cloud from Mt. Pinatubo 60 days after the eruption. The tracer has been set equal to 1 at grid points adjacent to the location of the volcano (15.1°N, 120.3°E) and at vertical levels 20 and 30 hPa and has been set equal to 0 elsewhere. In this figure, the mixing ratios have been multiplied by 1000 and the contour interval is 0.1. The numbers below the scheme labels are the peak zonal mean values for the gridded distributions. Particles in the trajectory calculations have been initialized within the same source region by means of a random number generator.

The age distribution computed with the short–time step version of the SLT in Fig. 3d suggests that time truncation errors in the SLT scheme are probably unimportant for the NCAR models. This does not, however, exclude the possibility that such errors contribute to the excessive numerical diffusion of the SLT scheme in the SKYHI model, owing to the latter's greater amount of short-term dynamical variability. Insufficient spatial and/or temporal resolution is also likely to affect the amount of numerical diffusion. For example, Figs. 8 and 9 show results from SKYHI runs similar to that shown in Fig. 7, but with vertical resolutions increased to 80 and 160 vertical levels (we note that this is not a clean test of the behavior of advection schemes with increasing vertical resolution, since the changes in resolution affect both tracer transport and dynamics). All four schemes produce less diffusive distributions (i.e., stronger gradients) with increasing resolution, but the contrast between the Eu-

lerian and the SLT distributions is somewhat reduced as the vertical resolution is increased. However, even with 150 vertical levels, the vertical spread is greater, the peak magnitude smaller, and the gradients weaker for the SLT than for the other schemes. Because all schemes should converge with increasing resolution, these results indicate that the convergence rate is much slower for the SLT scheme and that the scheme, when driven by winds produced by explicit dynamics with very short time steps, can produce unrealisticly young age distributions at the 2-km vertical resolution commonly used in contemporary GCMs. The contrast between $\dot{\sigma}$ and $\dot{\theta}$ trajectories discussed in section 5a suggests that all four schemes would produce less vertical transport if they were formulated in isentropic (rather than sigma) coordinates. For the SLT scheme, this modification may be relatively easy to implement. It would involve computing the SLT trajectories as $\dot{\theta}$ trajectories, possibly adopting parts of our online trajec-
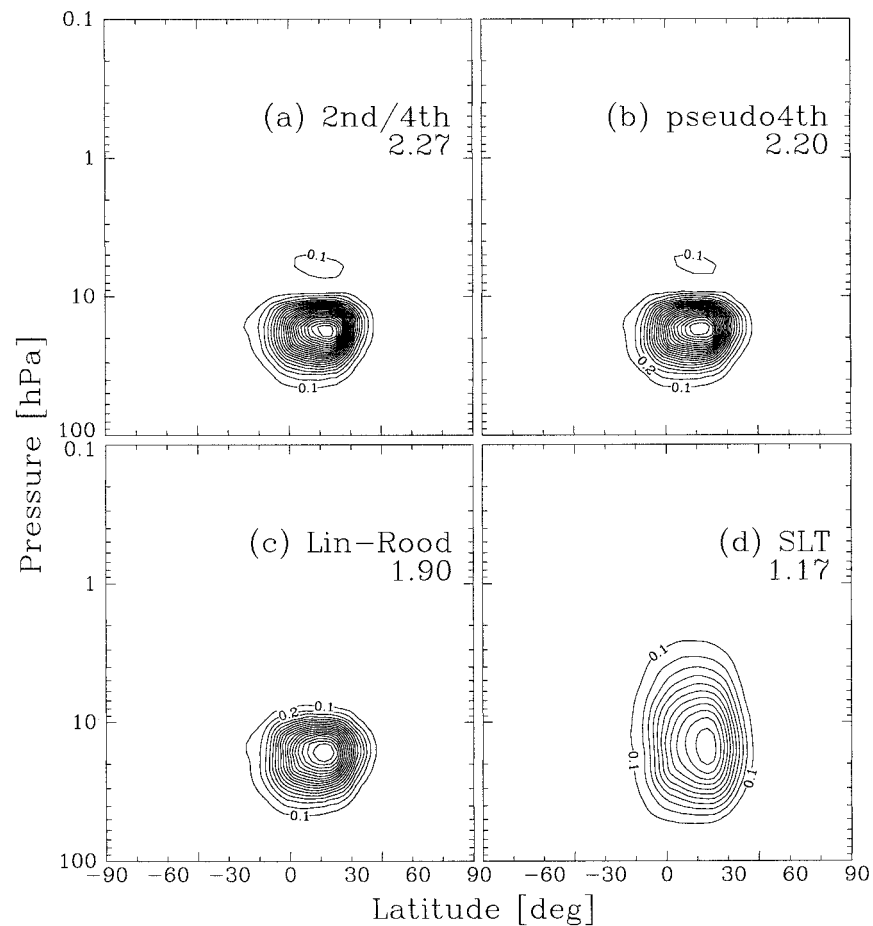
Fig. 8. Similar to Fig. 7, but from a SKYHI run with 80 vertical levels.

tory code. We plan to explore this possibility in the future.

The results from our Pinatubo runs seem consistent with the results obtained by Reames and Zapotocny (1999a,b), who compared the behavior of nine advection algorithms in shorter (48 h), but realistic, simulations with a channel model. In particular, Reames and Zapotocny determined that the centered difference schemes preserve the maxima of peaked distributions much better than a low-order version of the Lin–Rood scheme (FFSL-1 in the notation of Lin and Rood) and a variety of semi-Lagrangian schemes. However, they also confirmed the dispersion errors characteristic of the centered-difference schemes at higher wavenumbers and noted that these errors do not necessarily diminish with increasing resolution of the dynamical model. This is also clear from our results, for example, the presence of isolated 0.1 contours in Figs. 8a and 8b when the resolution is increased from 40 to 80 levels.

c. GEOS-2 results

To further ascertain that the diffusive nature of the SLT scheme is not peculiar to the SKYHI model, we have performed a Pinatubo-like simulation with the GEOS-2 model. The results from the GEOS-2 experiment are shown in Fig. 10. While the numerical values are different from those in Fig. 7, it is clear that the relative amount of numerical diffusion is similar: the 4th-order scheme is the least diffusive, while the SLT scheme is the most diffusive (judging by the gradients and maximum values; the extent of upward transport for the SLT scheme is not as great as in the SKYHI experiment). Based on these results, we conclude that the diffusive nature of the SLT scheme is general to explicit gridpoint GCMs, and that in such models the scheme will produce the youngest ages. We note that for the Lin–Rood scheme, we used a somewhat different version than in the SKYHI experiment (FFSL-3 in the horizontal and FFSL-5 in the vertical, without parameterized subgrid-scale mixing) and yet the difference between maximum mixing ratios in Figs. 10b and 10c (about 15%) is comparable to the difference between the pseudo–4th-order and Lin–Rood results in Fig. 7. Apparently, the amount of numerical diffusion for the Lin–Rood scheme, relative to the 4th-order scheme, is similar in the two cases (however, as shown in Fig. 2, the differences between different schemes in the Lin–
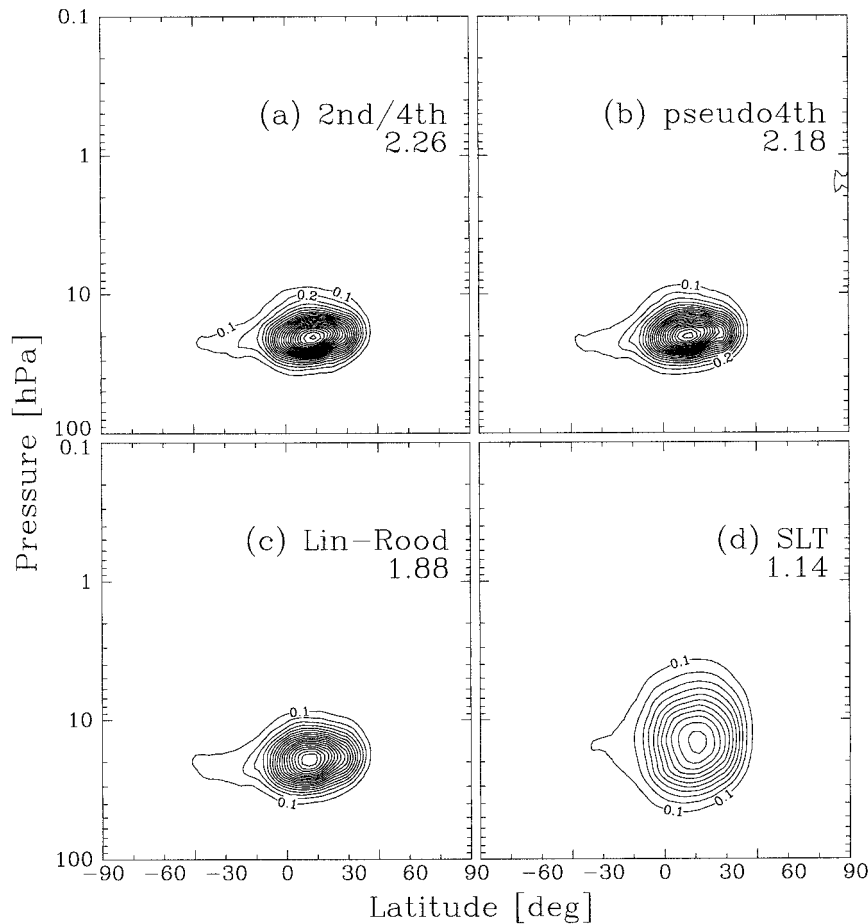
FIG. 9. Similar to Fig. 7, but from a SKYHI run with 160 vertical levels.

Rood hierarchy become more apparent in the multiyear age calculations).

6. Summary and discussion

Age-of-air calculations in a GCM can be extremely sensitive to the choice of advection scheme employed in solving the tracer continutity equation. This has been demonstrated in the GFDL SKYHI general circulation model using four gridded advection schemes (based on the model's $\dot\sigma$ velocities) and a Lagrangian trajectory code (which can utilize either $\dot\sigma$ or $\dot\theta$ velocities). A wide variety of age distributions, ranging from "peaked" to "flat" and from "young" to "old," has been obtained, depending on the choice of scheme, with the oldest and most realistic ages produced using the nondiffusive centered-difference schemes. The centered-difference schemes are capable, in particular, of producing ages older than 10 yr in the mesosphere and of eliminating the "young bias" found in previous age-of-air calculations. The ages computed using $\dot\theta$ trajectories are also in close agreement with the available observations, especially in high latitudes where the air is oldest. The

similarity of age distributions computed with the centered-difference schemes to the distribution obtained using $\dot\theta$ trajectories indicates that the lack of numerical diffusion in those schemes outweighs their dispersion errors in this application. The nonmonotonic version of the Lin–Rood scheme also produces a realistic-looking age distribution and a good match with observations in low and middle latitudes below 35 km, but in high latitudes and in the upper stratosphere, the nonmonotonic Lin–Rood ages are up to 3 yr younger than those obtained with the centered-difference schemes. Progressively younger ages are produced using monotonic versions of the Lin–Rood scheme. The sharpest contrast to the centered-difference schemes in the SKYHI model is provided by a semi-Lagrangian transport (SLT) scheme, which produces the youngest and clearly unrealistic ages. A special case is presented by the age distribution computed using $\dot\sigma$ trajectories. These trajectories exhibit spurious vertical displacements, which are inconsistent with the model's diabatic heating rates. These displacements appear to be a random walk phenomenon caused by high-frequency components in the computed $\dot\sigma$ velocities, including gravity waves and nu-
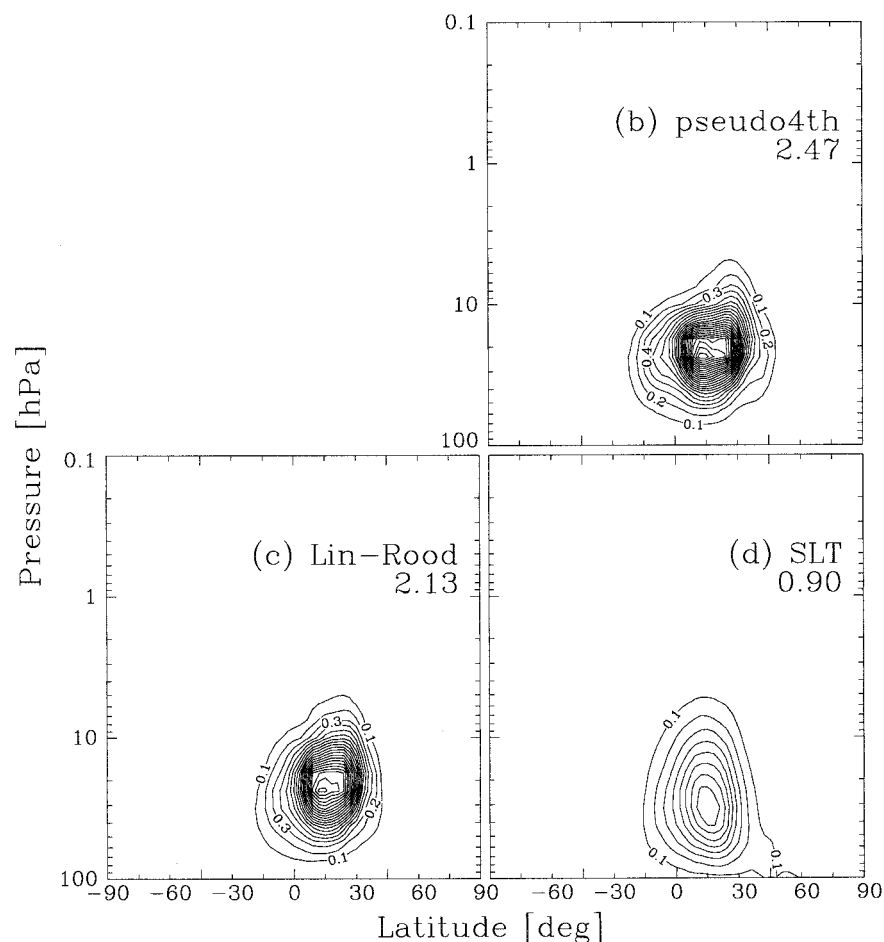
FIG. 10. Similar to Fig. 7, but for the GEOS-2 model.

merical noise, and they may also have been caused by the coarseness of the linear interpolation operator used in the trajectory code. Since these displacements occur in online calculations, they are not simply an aliasing problem. As a result of the spurious vertical displacements, the contours of mean age computed using $\dot\sigma$ trajectories exhibit weak vertical gradients and are unrealistic.

While at this stage we are unable to provide a definitive explanation for the very young SKYHI/SLT ages, they appear to be caused by interpolation errors related to SKYHI's short-term dynamical variability. This variability is produced by the short–time step, explicit, centered-difference dynamics employed in SKYHI (and similar GCMs) and is manifested in the gravity wave and mesoscale spectra (Hayashi et al. 1989; Koshyk et al. 1999a,b). Our online trajectory calculations, especially the contrast in the extent of vertical displacements between $\dot\sigma$ and $\dot\theta$ trajectories, suggest that numerical diffusion would be reduced if the SLT scheme were reformulated using $\dot\theta$ trajectories. We have also discovered that the SLT scheme in SKYHI shows signs of convergence to the other schemes as the vertical reso-

lution of the GCM is increased, but it appears to be more diffusive than the other schemes even at 0.5-km resolution. In comparison with the SKYHI/SLT ages, the ages computed using the SLT scheme in the MACCM3 are substantially older (albeit still rather young compared with observations) and they are rather insensitive to the length of time step adopted in solving the tracer continuity equation. This is most likely due to the MACCM3's use of a long–time step, semi-implicit, semi-Lagrangian dynamics, which reduces the dynamical variability and the associated interpolation errors.

Our results demonstrate that caution must be exercised in interpreting 3D age distributions solely in terms of a GCM's large-scale circulation field. At the same time, age appears to be useful in evaluating long-term diffusive properties of advection schemes (and possibly dynamical cores as well). It also seems obvious that in addition to age (and the ''age'' tracers such as CO_2 and SF_6), the choice of advection scheme will play an important role in the GCM simulations of other long-lived tracers, including N_2O, CH_4, and the CFCs. However, as those tracers are also affected by chemical and phys-

ical parameterizations, the effect of the choice advection scheme is likely to be reduced compared with stratospheric age (Hall et al. 1999). For example, no problems with the NCAR SLT scheme were evident in the multiyear tropospheric simulations of a CFC-11-1ike tracer by Pyle and Prather (1996) and Hartley et al. (1994), presumably because in those simulations the subgrid scale parameterized transport (both convective and in the planetary boundary layer) was also important.

Clearly, more effort is needed to gain a better understanding of the behavior of advection schemes in long-term atmospheric (and oceanic) simulations. The MACCM3 and 2D results described in this paper suggest that the choice of advection scheme becomes progressively less important for slowly varying circulations, thus pointing to experiments with varying degrees of dynamical variability as a fruitful venue for future work. Among possible tasks for further research are 1) testing the various schemes in SKYHI using time-averaged winds (to see whether reducing the high-frequency wind variability reduces the spread in age distributions evident in Fig. 1), 2) calculating the age distribution in the MACCM3 using the spectral scheme (to see whether an essentially nondiffusive scheme can generate substantially older ages in a semi-implicit GCM), and 3) testing the sensitivity of age calculations to the choice of dynamical core (GFDL's Flexible Modeling System, currently under development, will include different dynamical cores as options). In addition to age (i.e., stratospheric CO_2), the choice of advection scheme can be expected to affect simulations of tropospheric CO_2 in which 1% differences are important (e.g., Fan et al. 1998), and this provides just one example that the issues at stake are not merely technical.

REFERENCES

Andrews, D. G., J. D. Mahlman, and R. W. Sinclair, 1983: Eliassen–Palm diagnostics of wave-mean flow interactions in the GFDL SKYHI general circulation model. *J. Atmos. Sci.,* **40,** 2768–2784.

Bacmeister, J. T., D. E. Siskind, M. E. Summers, and S. D. Eckerman, 1998: Age of air in a zonally averaged two-dimensional model. *J. Geophys. Res.,* **103,** 11 263–11 288.

Bischof, W., R. Borchers, P. Fabian, and B. C. Kruger, 1985: Increased concentration and vertical distribution of carbon dioxide in the stratosphere. *Nature,* **316,** 708–710.

Boering, K. A., S. C. Wofsy, B. C. Daube, H. R. Schneider, M. Loewenstein, J. R. Podolske, and T. J. Conway, 1996: Stratospheric mean ages and transport rates from observations of carbon dioxide and nitrous oxide. *Science,* **274,** 1340–1343.

Boville, B. A., J. R. Holton, and P. W. Mote, 1991: Simulation of the Pinatubo aerosol in general circulation model. *Geophys. Res. Lett.,* **18,** 2281–2284.

Burridge, D. M., and J. Haseler, 1977: A model for medium range weather forecasting—Adiabatic formulation. European Centre for Medium-Range Weather Forecasts Tech. Rep. 4, 46 pp.

Daniel, J. S., and Coauthors, 1996: On the age of stratospheric air and inorganic chlorine and bromine release. *J. Geophys. Res.,* **101,** 16 757–16 770.

Eluszkiewicz, J., 1996: A three-dimensional view of the stratosphere-to-troposphere exchange in the GFDL SKYHI model. *Geophys. Res. Lett.,* **23,** 2489–2492.

——, R. A. Plumb, and N. Nakamura, 1995: Dynamics of wintertime stratospheric transport in the Geophysical Fluid Dynamics Laboratory SKYHI general circulation model. *J. Geophys. Res.,* **100,** 20 883–20 900.

——, and Coauthors, 1996: Residual circulation in the stratosphere and lower mesosphere as diagnosed from Microwave Limb Sounder data. *J. Atmos. Sci.,* **53,** 217–240.

——, D. Crisp, R. G. Grainger, A. Lambert, A. E. Roche, J. B. Kumer, and J. L. Mergenthaler, 1997: Sensitivity of the residual circulation diagnosed from the *UARS* data to the uncertainties in the input fields and to the inclusion of aerosols. *J. Atmos. Sci.,* **54,** 1739–1757.

Fan, S., M. Gloor, J. Mahlman, S. Pacala, J. Sarmiento, T. Takahashi, and P. Tans, 1998: A large terrestrial carbon sink in North America implied by atmospheric and oceanic carbon dioxide data and models. *Science,* **282,** 442–446.

Fels, S. B., J. D. Mahlman, M. D. Schwarzkopf, and R. W. Sinclair, 1980: Stratospheric sensitivity to perturbations in ozone and carbon dioxide: Radiative and dynamical response. *J. Atmos. Sci.,* **37,** 2265–2297.

Hall, T. M., and R. A. Plumb, 1994: Age as a diagnostic of stratospheric transport. *J. Geophys. Res.,* **99,** 1059–1070.

——, and D. W. Waugh, 1997: Timescales for the stratospheric circulation derived from tracers. *J. Geophys. Res.,* **102,** 8991–9001.

——, ——, K. Boering, and R. A. Plumb, 1999: Evaluation of transport in stratospheric models. *J. Geophys. Res.,* **104,** 18 815–18 839.

Hamilton, K., R. J. Wilson, J. D. Mahlman, and L. J. Umscheid, 1995: Climatology of the SKYHI troposphere–stratosphere–mesosphere general circulation model. *J. Atmos. Sci.,* **52,** 5–43.

Harnisch, J., R. Borchers, P. Fabian, and M. Maiss, 1996: Tropospheric trends for CF_4 and C_2F_6 since 1982 derived from SF_6 dated stratospheric air. *Geophys. Res. Lett.,* **23,** 1099–1102.

——, ——, ——, and ——, 1999: CF_4 and the age of mesospheric and polar vortex air. *Geophys. Res. Lett.,* **26,** 295–298.

Hartley, D., D. L. Williamson, P. J. Rasch, and R. Prinn, 1994: An examination of tracer transport in the NCAR CCM2 by comparison of $CFCl_3$ simulations with ALE/GAGE observations. *J. Geophys. Res.,* **99,** 12 885–12 896.

Hayashi, Y., D. G. Golder, J. D. Mahlman, and S. Miyahara, 1989: The effect of horizontal resolution on gravity waves simulated by the GFDL ''SKYHI'' general circulation model. *Pure Appl. Geophys.,* **130,** 421–443.

Holton, J. R., 1986: A dynamically based transport parameterization for one-dimensional photochemical models of the stratosphere. *J. Geophys. Res.,* **91,** 2681–2686.

Kida, H., 1983: General circulation of air parcels and transport characteristics derived from a hemispheric GCM, Part 2, Very long-term motions of air parcels in the troposphere and stratosphere. *J. Meteor. Soc. Japan,* **61,** 510–522.

Kiehl, J. T., J. J. Hack, G. B. Bonan, B. A. Boville, B. P. Briegleb, D. L. Williamson, and P. J. Rasch, 1996: Description of the NCAR Community Climate Model (CCM3). NCAR Tech. Note NCAR/TN-420+STR, Boulder, CO, 152 pp.

——, ——, ——, ——, D. L. Williamson, and P. J. Rasch, 1998: The National Center for Atmospheric Research Community Climate Model: CCM3. *J. Climate,* **11,** 1131–1149.

Koshyk, J. N., B. A. Boville, K. Hamilton, E. Manzini, and K. Shibata, 1999a: Kinetic energy spectrum of horizontal motions in middle atmosphere models. *J. Geophys. Res.,* **104,** 27 177–27 190.

——, K. Hamilton, and J. D. Mahlman, 1999b: Simulation of the $k^{-5/3}$ mesoscale spectral regime in the GFDL SKYHI general circulation model. *Geophys. Res. Lett.,* **26,** 843–846.

Levy, H., II, J. D. Mahlman, and W. J. Moxim, 1982: Tropospheric N_2O variability. *J. Geophys. Res.,* **87,** 3061–3080.

Lin, S.-J., and R. B. Rood, 1996: Multidimensional flux-form semi-Lagrangian transport schemes. *Mon. Wea. Rev.,* **124,** 2046–2070.

Mahlman, J. D., 1997: Dynamics of transport processes in the upper troposphere. *Science,* **276,** 1079–1083.

——, and R. W. Sinclair, 1977: Tests of various numerical algorithms applied to a simple trace constituent air transport problem. *Fate of Pollutants in the Air and Water Environments,* I. H. Suffet, Ed., John Wiley & Sons, 223–252.

——, and W. J. Moxim, 1978: Tracer simulation using a global general circulation model: Results from a midlatitude instantaneous source experiment. *J. Atmos. Sci.,* **35,** 1340–1374.

——, H. Levy, and W. J. Moxim, 1986: Three-dimensional simulations of stratospheric N_2O: Predictions for other trace constituents. *J. Geophys. Res.,* **91,** 2687–2707.

Mote, P. W., J. R. Holton, and B. A. Boville, 1994: Characteristics of stratopshere–troposphere exchange in a general circulation model. *J. Geophys. Res.,* **99,** 16 815–16 829.

——, and Coauthors, 1996: The imprint of tropical tropopause temperatures on stratospheric water vapor. *J. Geophys. Res.,* **101,** 3989–4006.

Neu, J. L., and R. A. Plumb, 1999: The age of air in a ''leaky pipe'' model of stratospheric transport. *J. Geophys. Res.,* **104,** 19 243–19 255.

Plumb, R. A., 1996: A tropical pipe model of stratospheric transport. *J. Geophys. Res.,* **101,** 3957–3972.

Pollock, W. A., L. E. Heidt, R. A. Lueb, J. F. Vedder, M. J. Mills, and S. Solomon, 1992: On the age of stratospheric air and ozone depletion potentials in the polar regions. *J. Geophys. Res.,* **97,** 12 993–12 999.

Prather, M. J., 1986: Numerical advection by conservation of second-order moments. *J. Geophys. Res.,* **91,** 6671–6681.

Pyle, J., and M. Prather, 1996: Global tracer transport models. Report of a scientific symp., WMO/TD-No. 770, 186 pp.

Rasch, P. J., and D. L. Williamson, 1990: On shape-preserving interpolation and semi-Lagrangian transport. *SIAM J. Sci. Stat. Comput.,* **11,** 656–687.

——, X. Tie, B. A. Boville, and D. L. Williamson, 1994: A three-dimensional transport model for the middle atmosphere. *J. Geophys. Res.,* **99,** 999–1017.

Reames, F. M., and T. H. Zapotocny, 1999a: Inert trace constituent transport in sigma and hybrid isentropic–sigma models. Part I: Nine advection algorithms. *Mon. Wea. Rev.,* **127,** 173–187.

——, and ——, 1999b: Inert trace constituent transport in sigma and hybrid isentropic–sigma models. Part II: Twelve semi-Lagrangian algorithms. *Mon. Wea. Rev.,* **127,** 188–200.

Ritchie, H., 1991: Application of the semi-Lagrangian method to a multilevel spectral primitive-equations model. *Quart. J. Roy. Meteor. Soc.,* **117,** 91–106.

Rood, B. B., 1987: Numerical advection algorithms and their role in atmospheric transport and chemistry models. *Rev. Geophys.,* **25,** 71–100.

Russell, J. M., M. Luo, R. J. Cicerone, and L. E. Deaver, 1996: Satellite confirmation of the dominance of chlorofluorocarbons in the stratospheric chlorine budget. *Nature,* **379,** 526–529.

Schmidt, U., and A. Khedim, 1991: In situ measurements of carbon dioxide in the winter arctic vortex and at midlatitudes: An indicator of the age of stratospheric air. *Geophys. Res. Lett.,* **18,** 763–766.

Schubert, S. D., J. Pfaendtner, and R. Rood, 1993: An assimilated dataset for earth science applications. *Bull. Amer. Meteor. Soc.,* **74,** 2331–2342.

Shapiro, R., 1970: Smoothing, filtering and boundary effects. *Rev. Geophys. Space Phys.,* **8,** 359–387.

Shia, R.-L., M. K. W. Ko, D. K. Weisenstein, C. Scott, and J. Rodriguez, 1998: Transport between the tropical and mid-latitude lower stratosphere: Implications for ozone response to HSCT emissions. *J. Geophys. Res.,* **103,** 25 435–25 446.

Smagorinsky, J., 1963: General circulation experiments with the primitive equations. I. The basic experiment. *Mon. Wea. Rev.,* **91,** 99–164.

Smolarkiewicz, P. K., 1983: A simple positive definite advection scheme with small implicit diffusion. *Mon. Wea. Rev.,* **111,** 479–487.

Strahan, S. E., and J. D. Mahlman, 1994: Evaluation of the GFDL SKYHI general circulation model using aircraft N_2O measurements: 2. Tracer variability and diabatic meridional circulation. *J. Geophys. Res.,* **99,** 10 319–10 332.

Takacs, L. L., A. Molod, and T. Wang, 1994: Documentation of the Goddard Earth Observing System (GEOS) general circulation model—Version 1. NASA Tech. Memo. 104606, Vol. 1, Goddard Space Flight Center, Greenbelt, MD, 100 pp.

Volk, C. M., and Coauthors, 1997: Evaluation of source gas lifetimes from stratospheric observations. *J. Geophys. Res.,* **102,** 25 543–25 564.

Waugh, D. W., and Coauthors, 1997: Three-dimensional simulations of long-lived tracers using winds from MACCM2. *J. Geophys. Res.,* **102,** 21 493–21 513.

Weaver, C. J., A. R. Douglass, and R. B. Rood, 1993: Thermodynamic balance of three-dimensional stratospheric winds derived from a data assimilation procedure. *J. Atmos. Sci.,* **50,** 2987–2993.

Weisenstein, D. K., M. K. W. Ko, I. G. Dyominov, G. Pitari, L. Ricciardulli, G. Visconti, and S. Bekki, 1998: The effect of sulfur emissions from HSCT aircraft: A 2-D model intercomparison. *J. Geophys. Res.,* **103,** 1527–1547.

Williamson, D. L., and P. J. Rasch, 1989: Two-dimensional semi-Lagrangian transport with shape-preserving interpolation. *Mon. Wea. Rev.,* **117,** 102–129.

——, and ——, 1994: Water vapor transport in the NCAR CCM2. *Tellus,* **46A,** 34–51.

——, J. G. Olson, and B. A. Boville, 1998: A comparison of semi-Lagrangian and Eulerian tropical climate simulations. *Mon. Wea. Rev.,* **126,** 1001–1012.

Woodbridge, E. L., and Coauthors, 1995: Estimates of total organic and inorganic chlorine in the lower stratosphere from in situ and flask measurements during AASE II. *J. Geophys. Res.,* **100,** 3057–3064.